SIMULATION OF TURBULENT COMBUSTION IN A SMALL-SCALE OBSTRUCTED CHAMBER USING FLAMEFOAM

Jaseliūnaitė, J.[1] and Povilaitis, M.[2]
[1] Laboratory of Nuclear Installation Safety, Lithuanian Energy Institute, Breslaujos g. 3, Kaunas, LT-44403, Lithuania, justina.jaseliunaite@lei.lt
[2] Laboratory of Nuclear Installation Safety, Lithuanian Energy Institute, Breslaujos g. 3, Kaunas, LT-44403, Lithuania, mantas.povilaitis@lei.lt

ABSTRACT

Dynamic overpressures achieved during the combustion are related to the acceleration experienced by the propagating flame. In the case of premixed turbulent combustion in an obstructed geometry, obstacles in the direction of flow result in a complex flame front interaction with the turbulence generated ahead of it. The interaction of flame front and vortex significantly affect the burning rate, the rate of pressure rise and achieved overpressure, the geometry of accelerating flame front and resulting structures in the flow field.

Laboratory-scale premixed turbulent combustion experiments are convenient for the study of flame acceleration by obstacles in higher resolution. This paper presents numerical simulations of hydrogen-air mixture combustion experiments performed in the University of Sydney small-scale combustion chamber. The simulations were performed using flameFoam – an open-source premixed turbulent combustion solver, based on OpenFOAM. The experimental and numerical pressure evolutions are compared. Furthermore, flow structures, which develop due to the interaction between the obstacles and the flow, are investigated with different obstacle configurations.

1.0 INTRODUCTION

Currently hydrogen energy is preferred due to high efficiency and zero emissions operation. Hydrogen can deliver and store an enormous amount of energy. However, ignition energy of hydrogen is extremely low and there is huge risk to safety as it can provoke large explosive failures. Explosive hydrogen gas pose combustion safety hazards to many industries including but not limited to chemicals, electronics, metallurgy, textile fiber manufacturing, fuel for rocket launchers. Determination of the flame speed, overpressures, possibility for transition to detonation is important to adequate risk assessment for the safety.

Most hydrogen explosion cases occur in confined areas with obstructions, where flame experience expansion and compression and as a result it is accelerated and becomes turbulent. Thus, channels with obstacles are used to study the flame acceleration and turbulent combustion. Fairweather et al. [1] experimentally and theoretically investigated flame shape and generated overpressures in cylindrical vessels with turbulence-inducing rings. They found that premixed flame just after propagating though the vent became rapidly turbulent due to flame front interaction with the obstacles leading to high overpressures, before that flame was substantially laminar. The data reported by Chen et al. [2] indicate that investigated flame shape in an obstructed tube can be categorized with regard to propagation evolution stages into: spherical flame, finger-like shaped flame, jet flame, mushroom-shaped flame and bidirectional propagation flame. Moreover, flame shape can be explained by pure hydrodynamics, more precisely flame-vortex interaction. In another work, Chen el at. [3] again investigated flame propagation in an obstructed chamber but this time with two slits. Nevertheless, the flame propagation can be divided into same stages as mentioned before, but without mushroom-shaped flame, since flame has to propagate though two slits, which results in the twin jet flames. These twin jet flame also have their patterns for example, the merged flames, paralleling jet flames and separated jet flames.

In the subsequent detailed numerical studies, Qin et al. [4] explored the premixed flame propagation in a closed duct with obstacles, reported that higher number of obstacles give rise to the stronger Rayleigh-Taylor and Kelvin-Helmholtz instabilities, this implies greater turbulence and more obvious flame stretching. Furthermore, it was found that flame structure change over time from spherical to finger flame before passing obstacles and mushroom-like flame after it is deformed due to transition from laminar to turbulent flame. Later flame front evolves into a twisted flame and afterwards becomes the plane flame or the finger flame when obstacles are no longer encountered. Another important finding from Fan et al. [5] is that the flame shape and flame propagation process are mainly determined by flow velocity. Moreover, they concluded that turbulent flow folds, bends and stretches surface area of flame, therefore flame accelerates, but at some point, turbulent flame speed reaches a limit and turbulent combustion has no effect on the flame acceleration and becomes stable. Reports made by Wang et al. [6], Wen et al. [7] and Xiao et al. [8] indicated that the flame velocity increases abruptly when the flame goes through an obstruction, besides the sharper interaction between flame front and obstacle, the higher the peak overpressure.

However, flame structure and propagation investigation in obstuctured geometries is still a very difficult research topic because the flame shape and the flame-vortex interaction of accelerated turbulent combustion is mostly inaccessible to experimental measurement. Although combustion in confined areas with obstructions is a crucial issue in the safety of industrial processes, experimental and numerical studies are still needed in order to provide knowledge that is useful to predicting and understanding the effects of obstacles and complex geometries in the flame propagation and development process.

The objective of the present study is investigation of flame propagation and developed flame structure due to the interaction between the obstacles and the flow. For simulation flameFoam solver based on Reynolds-averaged Navier-Stokes equations along with transport equation for a progress variable was used. The validation of model was based on the overpressures generated in the laboratory-scale chamber [9] having different configurations of obstacles.

2.0 METHODOLOGY

2.1 The laboratory-scale chamber

Combustion experiment in the laboratory-scale chamber conducted by Al-Harbi [9] was referred to validate the model in this study. The experiment setup was composed of 50 × 50 × 250 mm chamber. Three removable aluminium baffle plates of 0.4 area blockage were located vertically starting from 19 mm from the ignition source at the base of chamber and a spacing distance of 30 mm. Baffle consists of five 4 mm wide and 3 mm thick strips separated by 5 mm gaps. Furthermore, chamber have a solid square obstacle of 12 mm or 25 mm in cross-section, which is located at 96 mm from the ignition point. Due to the ability to rearrange the baffle plates the flame speed and the flame front can be controlled as well as turbulence intensity, also flow structure can be investigated in several different configurations.

The top of the chamber is opened moment before combustions starts, before it mixture of hydrogen and air is injected though a non-return valve at atmospheric pressure and the mixture is left to settle. The mixture is ignited by focussing the infrared output from a Nd:YAG laser 2 mm above the base. Two Keller type PR21-SR pjezo-electric pressure sensors are placed at the base of the chamber and 64 mm from the chamber top in the wall.

2.2 flameFoam

Simulations were performed using a custom-built solver – flameFoam, developed using OpenFOAM toolkit. It is publicly hosted on https://github.com/flameFoam/flameFoam. The premixed combustion is governed by equations for conservation of mass, momentum and energy, respectively:

$$\frac{\partial \rho}{\partial t} + \Delta \cdot \left(\rho \vec{U}\right) = 0 \tag{1}$$

$$\frac{\partial \rho \vec{U}}{\partial t} + \Delta \cdot \left(\rho \vec{U} \times \vec{U}\right) = \nabla \cdot \tau_{eff} - \nabla p + \rho \vec{g} \tag{2}$$

$$\frac{\partial \rho h}{\partial t} + \Delta \cdot \left(\rho \vec{U} h\right) + \frac{\partial \rho K}{\partial t} + \Delta \cdot \left(\rho \vec{U} K\right) = \frac{\partial p}{\partial t} + \nabla \cdot \left(\alpha_{eff} \nabla h\right) + \rho\left(\vec{g} \cdot \vec{U}\right) + S_h(S_c) \tag{3}$$

where: ρ – density, kg/m^3; t – time, s; U – velocity, m/s; τ_{eff} – shear stress, N/m^2; p – pressure, Pa; g – gravitational acceleration, m/s^2; h – enthalpy, J; K – kinetic energy, J; α_{eff} – effective thermal diffusivity, m^2/s; S_h – enthalpy source, S_c – combustion source.

Also, a transport equation for a progress variable c is included to model combustion process, it is closed using source term introduced by Zimont [10]:

$$\frac{\partial \rho c}{\partial t} + \Delta \cdot \left(\rho \vec{U} c\right) = \nabla \cdot \left(\frac{\mu_{Eff}}{Sc_T} \nabla c\right) + S_c \tag{4}$$

$$S_c = \rho_u S_T |\nabla c| \tag{5}$$

where: c – progress variable; μ_{eff} – effective dynamic viscosity, m^2/s; S_T – turbulent flame speed, m/s.

Progress variable is defined as:

$$c = \frac{Y_0^{H_2} - Y^{H_2}}{Y_0^{H_2} - Y_\infty^{H_2}} \tag{6}$$

where: $Y_0^{H_2}$– initial hydrogen mass fraction; Y^{H_2} – hydrogen mass fraction; $Y_\infty^{H_2}$ – final hydrogen mass fraction

Progress variable acquires value of 0 when mixture is unburned and value of 1 when mixture is fully burned. Moreover, c can get intermediate values, which are within the flame brush.

The Bradley turbulent flame speed model was employed to close Equation (4). Therefore, the turbulent flame speed was calculated from the following equation [11]:

$$S_T = u' 0.88 (Ka\ Le)^{-0.3} \tag{7}$$

where: S_t – turbulent flame speed, m/s; u‘– RMS velocity, m/s; Ka – Karlovitz stretch factor; Le – Lewis number.

Where fluctuating velocity:

$$u' = \left(\frac{2}{3} k\right)^{\frac{1}{2}} \tag{8}$$

where: k – turbulent kinetic energy, J/kg.

Karlovitz stretch factor has the following form [11]:

$$Ka = 0.157 \left(\frac{u'}{S_L}\right)^2 Re_T^{\frac{-1}{2}} \tag{9}$$

$$Re_T = \frac{u' l_t^B}{\nu} \tag{10}$$

$$l_t^B = \left(\frac{3}{2}\right)^{\frac{3}{2}} \frac{u'^3}{\varepsilon} \tag{11}$$

where: S_L – laminar flame speed, m/s; Re_T – turbulent Reynolds number; ν – kinematic viscosity, m^2/s; l_t^B – Bradley turbulent length scale, m; ε – turbulent dissipation rate, m^2/s^3.

Validation of the presented model and flameFoam implementation has been performed on several experiments of turbulent premixed hydrogen-air experiments. Sensitivity analyses based on ENACCEF experimental facility tests were done in [12]. Additionally, model has been blindly validated in the on-going ETSON-SAMHYCO-NET benchmark with good results.

2.3 Initial and boundary conditions and computational details

The calculations were performed using initial values and model constants described in Table 1. All simulations were performed with Euler time discretization scheme. A second order discretization schemes were used for convective, diffusive terms, progress variable and turbulence parameters, for enthalpy VanLeer divergence discretization scheme was used. Time step was automatically adjusted by Courant number which was set to maximum value of 0.75. *k-ω SST* turbulence model with standard turbulence boundary conditions was used. Turbulent kinetic energy and dissipation rate are calculated by *k-ω SST* turbulence model from its balance equation system [13].

Table 1. Initial conditions and constants

Initial conditions		
Pressure	p	10^5 kg/m s^2
Temperature	T	293 K
Initial hydrogen volume fraction	X_{H2}	0.2265
Laminar flame speed	S_{L0}	1.16 m/s
Turbulence parameters	k, ω	Extremely low values
Model constants		
Turbulent Scmidt number	Sc_T	0.9
Lewis number	Le	0.5

The computational domain measures 50 × 25 × 250 mm for the chamber as it has symmetry wall in y-z plane, any other symmetry planes were not used. Also, the domain has an additional extension at the end of the chamber in x and y direction by 30 mm also in z direction by 100 mm with the outlet boundary conditions. The walls and obstacles of the chamber have adiabatic and no-slip boundary conditions. A total of 4 configurations using different combinations of baffles and obstacles were selected for research: BBBS, BB0S, BBBL and BB0L, for example, BBB employs three consecutive baffles, where fourth symbol means whether it will be small (S) or large (L) obstacle (see chapter 2.1 for obstacle dimensions). One of computational domain is shown in Fig. 1.

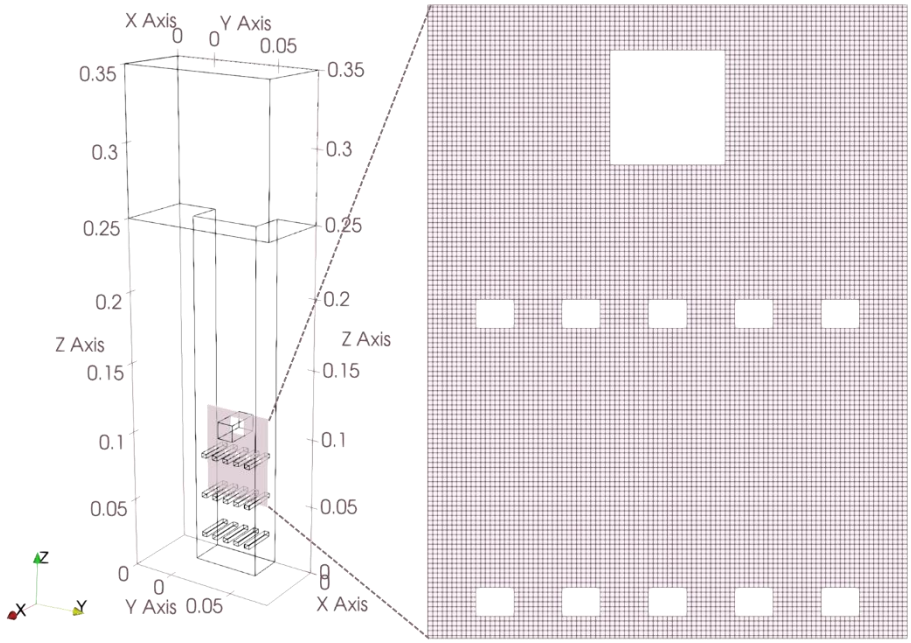

Figure 1. Computational domain and mesh of BBBS configuration

Ignition is provided by initializing a burned flame spherical area which have radius equal to 0.007 m and progress variable value of 1. As ignition was set at the base of the chamber its shape is hemispherical.

Tree-dimensional simulation was carried out using two numerical grids in order to examine solution dependence on grid resolution. First grid cell size is equal to 1 mm having 866200 cells, second grid cell size is equal to 0.5 mm having 6845200 cells. For comparison was selected flame shape rather than pressure values, as ignition radius is not equal in both simulations. The flame front structure for several moments is compared in Fig. 2. There are no significant differences in the flame front structure except that the denser mesh is capable of giving finer details than coarse. Whereas the purpose of this study is to investigate the structure of the flame front, this can be done with much greater detail using denser grid. Therefore, in further research finer mesh was used.

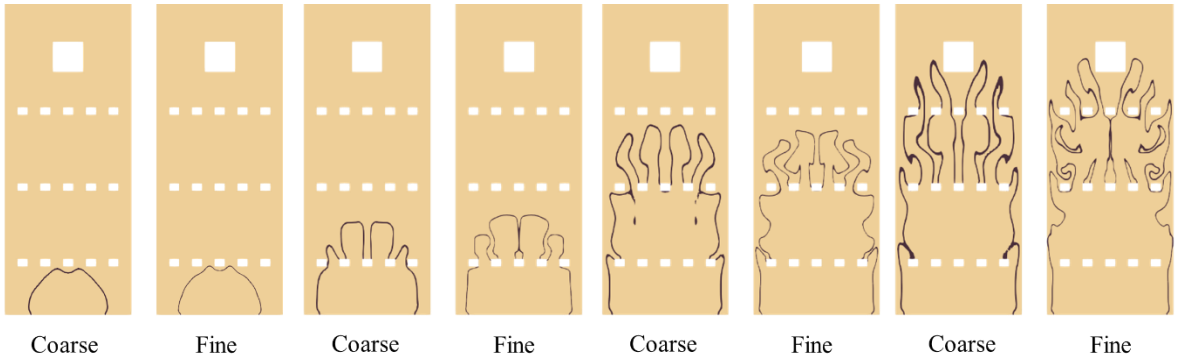

Figure 2. Comparison of coarse and fine mesh frame fronts

3. RESULTS AND DISSCUSION

3.1. Overpressure evolution

Overpressure results of all configurations can be seen in Fig. 3. Pressure was measured in the centre of the chamber base. Both numerical and experimental overpressures increase slowly until t = 0.003 s, which is due to laminar combustion. After that despite the obstacles configuration the overpressure increases abruptly. The significant increase of pressure occurs when the flame surface area increases because of passage through baffles, therefore turbulent flame propagation starts.

Without the third baffle and with a small obstacle (BB0S) the maximum reached overpressure decrease drastically compared to BBBS, whereas configurations with large obstacle manage to maintain overpressure even after removal of the baffle. Numerical simulations were more sensitive to change from BBBS to BB0S, than change from BBBL to BB0L. A large obstacle resulted in a higher blockage ratio, whereas removal of one baffle was not significant for the modelled overpressure. Furthermore, removal of third baffle led to peak overpressure delay since peak value is obtained when the flame front reaches the exit of the chamber, whereas less turbulence is generated in BB0L and BB0S configurations, resulting in a slower flame propagation. After the flame front escapes chamber pressure drops significantly to atmospheric level due to venting.

Overall, the numerical calculations give good prediction for cases such as BBBS, BB0S and BBBL despite a small degree of under-estimation or over-estimation of the overpressure magnitude. BB0L has higher pressure peak than expected, this occurs due to excessive turbulence.

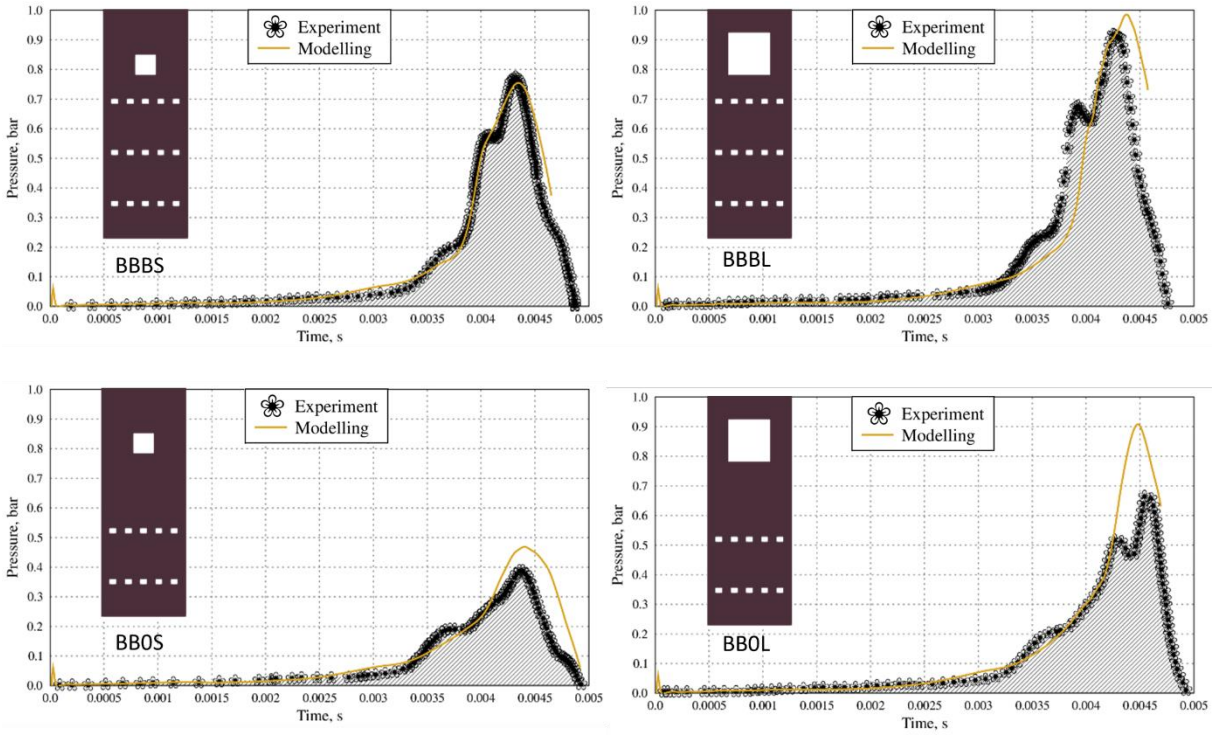

Figure 3. Evolution of overpressures

3.2. Flame shape characteristics and the configuration change analysis

A sequence of premixed flame propagation for the hydrogen/air mixture in the small-scale chamber with a different configuration of obstacles is given in Fig. 4. The flame structure at first shown moment is hemi-spherical in all cases, and the flame starts to expand and elongate in axial direction.

As the flow encounters the first baffle, laminar flame front is distorted due to unstable deformation and transforms into a turbulent flame. The flame front protrudes though the narrow vents thus creating finger-like shaped flame front. The flame shape until t = 3.5 ms is almost the same in all configurations. Thin flame fronts wrap around the first and the second baffle plates thus trapping some of the unburn mixture above obstructions, where vortices are generated.

The flame front differences are observed depending on whether the flame interacts (BBBS, BBBL) or does not (BB0S, BB0L) with the third baffle plate. Until that moment flame already became progressively accelerated as a consequence of squeezing and stretching, but interaction with one more baffle generates even more turbulence. Comparing flame velocities and the flame front position (BBBS with BB0S and BBBL with BB0L) shows that more obstacles result in increased level of turbulence and faster combustion process.

Furthermore, the absence of third baffle lets finger-like structures to merge in the middle of chamber (t = 3.75 ms), whereas the third baffle keeps flame front distorted in the individual fingers. For configurations BBBS and BB0S with a small obstacle, propagating flame maintains more uniform velocity around the main obstacle, whereas large obstacle in BBBL and BB0L configurations causes abrupt gradients of velocity near the walls (t = 4 ms). After the flame front reaches main obstacle, higher amount of the unburned mixture upstream of the square obstacle is trapped in cases with the third baffle, because flame was greatly wrinkled. On the other hand, higher amount of the unburned mixture downstream of the square obstacle was trapped in cases with no third baffle (t = 4.25, 4.5 ms). After propagating though the last obstacle the flame is expanded and accelerated, therefore the flame front reconnects after crossing over the square obstacle and forms tulip shape flame front which later.

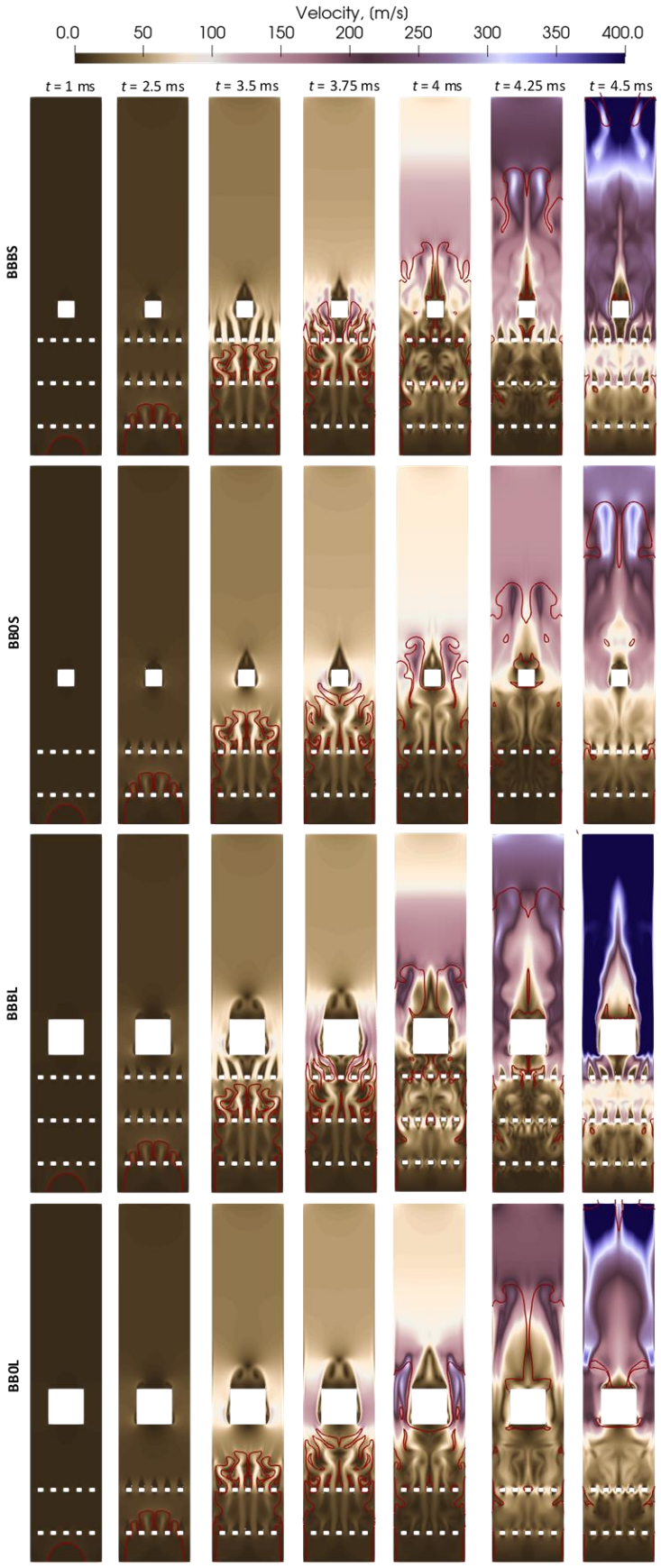

Figure 4. Numerical snapshots of the velocity fields with flame front represented by the red iso-line of $c = 0.5$

3.3. Coupling effect between flame and vortex

Vortex interaction with the flame control the evolution of flame structure as well as increases combustion rate and turbulence intensity. Fig. 5 shows the relation between flame front structure and vortices. As seen from Fig. 5 vortices represented by the second invariant of velocity gradient tensor are distributed just after obstacles in all chamber, while those nearby the flame front decay as a result of flame expansion and viscosity increase. Some eddies can be seen behind the flame front modifying its structure by perturbing its propagation. In Fig. 5 zoomed view stretching of finger-like shaped flames by vortices behind (internal perturbation) and in front of (external perturbation) the flame can be observed, the latter results in vortex entrainment. In addition, the core of flame is full of vortices, which enhance mixing of reacted mixture with some trapped unburned mixture.

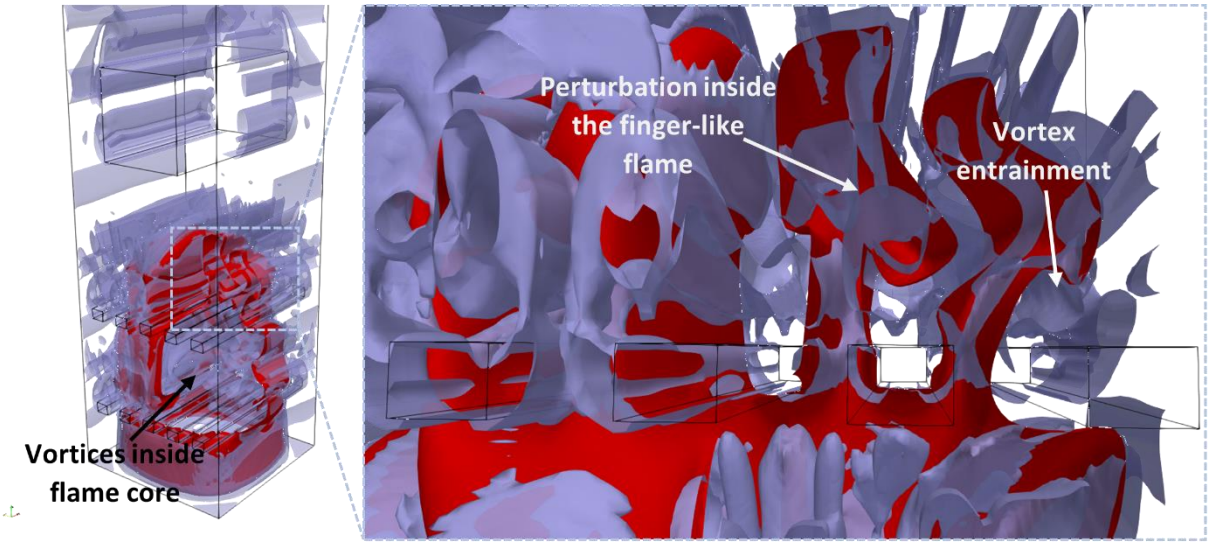

Figure 5. Flame front represented by the iso-surface of c = 0.5 (red) and iso-surface of the second invariant of the velocity gradient tensor (blue) (BB0L configuration, t = 34 ms)

Also, in Fig. 6 bidirectional propagation flame was observed and it is caused by vortex-flame interaction, where flame front propagates upwards, but due to interaction is directed downwards by swirling motion. This happens mainly in the wake of obstructions, where strong recirculation zones are created due to high turbulence. Reacting flame front flow is entrained into the vortex core due to high vorticity. This phenomenon increases the flame speed along with promotion of the consumption rate of the reactants, which enhance volumetric expansion.

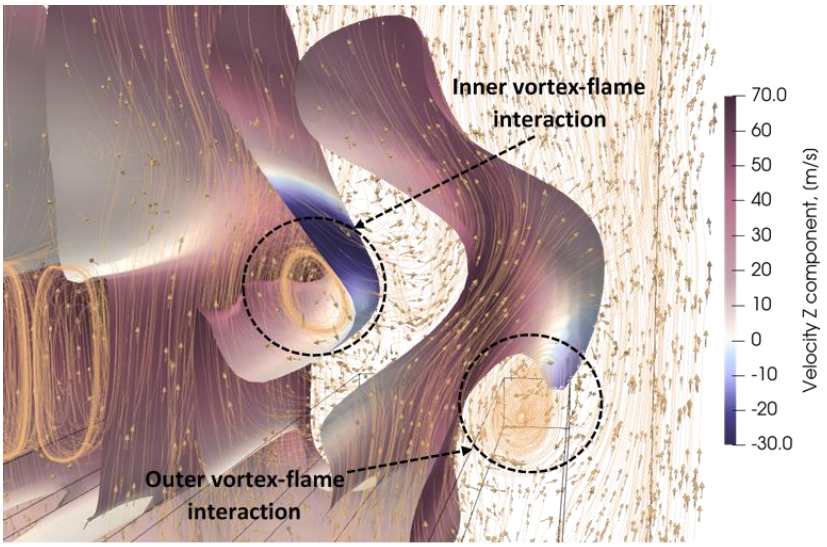

Figure 6. Velocity z component mapped onto iso-surface of flame front (c = 0.5) together with flow streamlines (BB0L configuration, t = 34 ms)

4. CONCLUSIONS

This paper presents numerical study on the premixed combustion of hydrogen/air mixture and flame propagation in a vented chamber under different obstacle configurations. The main findings are as follows:

1. The overpressures from ignition to flame passage through the exit of the chamber undergoes slow growth, turbulent growth and sudden drop. Also, a large square obstacle maintains overpressure peak value, while a configurations with a small obstacle are more affected by baffle changes. Numerical prediction shows reasonable agreement considering used simplified combustion model.

2. The flame front protrusion through the obstacles indicate regime transition from laminar to turbulent due to the flow compression and flame front stretching. Further propagation through baffles and obstructions results in gradually increasing turbulence degree. The corresponding flame propagation stages are hemi-spherical, finger-like, and finally, tulip. Besides, bidirectional flame propagation was observed where vortices interacted with the flame.

3. Vortex-flame interaction was observed both from the front and behind the flame, resulting in external and internal perturbations, respectively. Regardless of the vortex, vortex-flame interaction wrinkles and stretches flame front, thus enhancing mixing as well as increasing turbulence intensity.

REFERENCES

1. Fairweather, M., Hargrave, G. K., Ibrahim, S. S., and Walker, D. G., Studies of premixed flame propagation in explosion tubes, *Combustion and Flame*, **116**, No. 4, 1999, pp. 504-518.
2. Chen, P., Guo, S., Li, Y., and Zhang, Y., Experimental and LES investigation of premixed methane/air flame propagating in a tube with a thin obstacle, *Combustion Theory and Modelling*, **21**, No. 2, 2017, pp. 274-292.
3. Chen, P., Sun, Y., Li, Y., and Luo, G., Experimental and LES investigation of premixed methane/air flame propagating in an obstructed chamber with two slits, *Journal of Loss Prevention in the Process Industries*, **49**, 2017, pp. 711-721.
4. Qin, Y., and Chen, X., Flame propagation of premixed hydrogen-air explosion in a closed duct with obstacles, *International Journal of Hydrogen Energy*, **46**, No. 2, 2021, pp. 2684-2701.

5. Fan, W. P., Gao, Y., Zhang, Y. M., Chow, C. L., and Chow, W. K., Numerical studies on turbulent flame propagation in premixed gas deflagration inside a tube. *Building simulation*, **13**, No. 4, 2020, pp. 849-864.
6. Wang, C., Cui, Y., Mebarki, A., and Cai, Y., Effect of a Tilted Obstacle on the Flame Propagation of Gas Explosion in Case of Low Initial Pressure. *Combustion Science and Technology*, 2020, pp. 1-18.
7. Wen, X., Ding, H., Su, T., Wang, F., Deng, H., and Zheng, K., Effects of obstacle angle on methane–air deflagration characteristics in a semi-confined chamber. *Journal of Loss Prevention in the Process Industries*, **45**, 2017, pp. 210-216.
8. Xiao, H., and Oran, E. S., Flame acceleration and deflagration-to-detonation transition in hydrogen-air mixture in a channel with an array of obstacles of different shapes. *Combustion and Flame*, **220**, 2020, pp. 378-393.
9. Al-Harbi AA. Turbulent premixed flames propagating past repeated obstacles. Ph.D. Thesis. *The University of Sydney*, 2013
10. Zimont, V., Polifke, W., Bettelini, M., and Weisenstein, W., An efficient computational model for premixed turbulent combustion at high Reynolds numbers based on a turbulent flame speed closure, *Journal of Engineering for Gas Turbines and Power*, **120**, No. 3, 1998, pp. 526-532.
11. Lipatnikov, A. N., and Chomiak, J., Turbulent flame speed and thickness: phenomenology, evaluation, and application in multi-dimensional simulations. *Progress in energy and combustion science*, **28**, No. 1, 2002, pp. 1-74.
12. Jaseliūnaitė, J., Povilaitis, M., Simulation of ENACCEF2 Premixed Hydrogen-Air Mixture Deflagration Experiment Using OpenFOAM. In: *International Conference on Nuclear Engineering*. American Society of Mechanical Engineers, **83785**, 2020. p. V003T12A014.
13. Menter, F. R., Kuntz, M., and Langtry, R., Ten Years of Industrial Experience with the SST Turbulence Model, Turbulence, Heat and Mass Transfer. *Turbulence, heat and mass transfer*, **4**, No. 1, 2003, pp. 625-632.